Restructured endoplasmic reticulum generated by mutant amyotrophic lateral sclerosis-linked VAPB is cleared by the proteasome

Giulia Papiani[1,*], Annamaria Ruggiano[1,*,‡], Matteo Fossati[1], Andrea Raimondi[3], Giovanni Bertoni[2,§], Maura Francolini[1], Roberta Benfante[1], Francesca Navone[1,¶] and Nica Borgese[1,4,§,¶]

[1]Consiglio Nazionale delle Ricerche Institute of Neuroscience and Department of Pharmacology, University of Milan, Milano, Italy
[2]Department of Nanochemistry, The Italian Institute of Technology, Genova, Italy
[3]Department of Neuroscience and Brain Technology, The Italian Institute of Technology, Genova, Italy
[4]Department of Health Science, University of Catanzaro "Magna Graecia", Roccelletta di Borgia (CZ), Italy

*These authors contributed equally to this work
‡Present address: Parc de Ricerca Biomedica de Barcelona (PRBB), 08003 Barcelona, Spain
§Present address: Consiglio Nazionale delle Ricerche, Institute of Materials for Electronics and Magnetism, Parma, Italy
¶Authors for correspondence (n.borgese@in.cnr.it; f.navone@in.cnr.it)

Summary

VAPB (vesicle-associated membrane protein-associated protein B) is a ubiquitously expressed, ER-resident tail-anchored protein that functions as adaptor for lipid-exchange proteins. Its mutant form, P56S-VAPB, is linked to a dominantly inherited form of amyotrophic lateral sclerosis (ALS8). P56S-VAPB forms intracellular inclusions, whose role in ALS pathogenesis has not yet been elucidated. We recently demonstrated that these inclusions are formed by profoundly remodelled stacked ER cisternae. Here, we used stable HeLa-TetOff cell lines inducibly expressing wild-type VAPB and P56S-VAPB, as well as microinjection protocols in non-transfected cells, to investigate the dynamics of inclusion generation and degradation. Shortly after synthesis, the mutant protein forms small, polyubiquitinated clusters, which then congregate in the juxtanuclear region independently of the integrity of the microtubule cytoskeleton. The rate of degradation of the aggregated mutant is higher than that of the wild-type protein, so that the inclusions are cleared only a few hours after cessation of P56S-VAPB synthesis. At variance with other inclusion bodies linked to neurodegenerative diseases, clearance of P56S-VAPB inclusions involves the proteasome, with no apparent participation of macro-autophagy. Transfection of a dominant-negative form of the AAA ATPase p97/VCP stabilizes mutant VAPB, suggesting a role for this ATPase in extracting the aggregated protein from the inclusions. Our results demonstrate that the structures induced by P56S-VAPB stand apart from other inclusion bodies, both in the mechanism of their genesis and of their clearance from the cell, with possible implications for the pathogenic mechanism of the mutant protein.

Key words: Inclusion bodies, Organized smooth ER, Neurodegenerative diseases, Tail-anchored proteins, Ubiquitination

Introduction

Intracellular inclusion bodies (IBs) generated by the accumulation of aggregated malfolded mutant proteins are a common feature of neurodegenerative pathologies such as amyotrophic lateral sclerosis (ALS) and Alzheimer's, Parkinson's and Huntington's diseases (Selkoe, 2003). Protein aggregation occurs when the amounts of malfolded or incompletely folded proteins exceed the capacity of the ubiquitin-proteasome system (UPS), and IB formation occurs when the protein aggregates become large enough to be visible at light microscope resolution (Kopito, 2000).

Although the link between protein aggregation and disease has been recognized for many years, the exact role of IBs in cellular degeneration is still incompletely understood and has turned out to be quite complex. On the one hand, by sequestering functional proteins, IBs can be toxic to cells (Olzscha et al., 2011). In particular, recruitment of UPS components to the ubiquitinated mutant protein aggregates perturbs protein homeostasis (Balch et al., 2008; Bence et al., 2001; Ross and Pickart, 2004). On the other hand, sequestration into IBs of small, submicroscopic, aggregates, which are thought to be highly toxic, can be

cytoprotective (Arrasate et al., 2004; Douglas et al., 2008; Tanaka et al., 2004). One potentially important factor contributing to the Jekyll and Hyde characteristics of IBs may be the ease of their elimination, with a higher toxicity expected for IBs that are difficult to clear. Of the two main cellular degradation pathways, the UPS or autophagy, the latter plays the dominant role in IB elimination (Fortun et al., 2003; Olzmann and Chin, 2008; Ravikumar and Rubinsztein, 2004). The bulk sequestration of IBs into autophagosomes avoids the need to extract and unfold each single substrate molecule, a prerequisite for access to the narrow proteasomal channel (Finley, 2009).

An unusual type of inclusion is generated by mutant forms of the protein VAMP-associated protein-B (VAPB). VAPB and its homologue VAPA are tail-anchored proteins of the Endoplasmic Reticulum (ER), consisting in an N-terminal cytosolic domain homologous to the nematode major sperm protein (MSP), a coiled-coil domain, and a C-terminal hydrophobic stretch, which serves as membrane anchor. The VAPs are adaptor proteins involved in a variety of important functions, among which membrane traffic, ER interaction with microtubules, the unfolded

protein response, and lipid transport mediated by exchange proteins (reviewed in Lev et al., 2008). Many of these functions are mediated by the ability of the cytosolic domain to recruit ligand proteins bearing the so-called FFAT motif [two phenylalanines in an acidic tract (Kaiser et al., 2005; Loewen and Levine, 2005; Loewen et al., 2003)].

VAPB is the product of one of the 10–13 genes that have been causally linked to familial amyotrophic lateral sclerosis (FALS) (reviewed by Andersen and Al-Chalabi, 2011), a lethal disease, characterized by degeneration of upper and lower motor neurons. A dominant missense mutation, resulting in substitution of proline 56 with serine in the MSP domain (P56S mutation), was identified in patients from eight related Brazilian families of Portuguese origin (Nishimura et al., 2005; Nishimura et al., 2004) and then in patients from an unrelated German family (Funke et al., 2010). Subsequently, another mutation (T46I) in the MSP domain was identified in a patient in the United Kingdom (Chen et al., 2010). Both the P56S and the T46I mutant proteins aggregate and form inclusions in transfected cells (Nishimura, 2004; Prosser et al., 2008; Teuling et al., 2007). Structural studies have revealed that P56 of the wild-type (wt) protein adopts the unusual *cis*-peptide bond conformation and that introduction of a *trans* bond by substitution with serine results in gross misfolding of the MSP domain (Shi et al., 2010). The misfolded MSP domain induces homo-aggregation, which involves also the coiled-coil and transmembrane domains (Kim et al., 2010; Suzuki et al., 2009).

In a previous study, we characterized the biogenesis and structure of P56S-VAPB inclusions (Fasana et al., 2010). We found that the newly synthesized mutant protein inserts normally into the ER membrane, where it rapidly clusters. These clusters than coalesce into larger paranuclear structures. At variance with all other IBs linked to neurodegenerative disorders, mutant VAPB inclusions correspond to domains of dramatically restructured ER that contain all of the mutant protein and that consist of ribbons of stacked cisternae interleaved by an electron-dense cytosolic layer of uniform width.

Here, we have investigated how cells handle these unusual inclusions. Unexpectedly, we find that the P56S-VAPB inclusions are efficiently cleared by the proteasome in a process involving at least one component of the ER-associated degradation (ERAD) machinery (Bernasconi and Molinari, 2011). We discuss the implications of these results for the pathogenic mechanisms of mutant, ALS-linked, VAPB.

Results

Restructured ER domains generated by P56S-VAPB in transiently transfected and stably expressing cell lines

As previously demonstrated, P56S-VAPB expressed in transiently transfected cells segregates to restructured ER domains in the juxtanuclear region that consist of tightly apposed smooth-surfaced cisternae separated by an electron-dense layer (Fasana et al., 2010) (Fig. 1A,B). To gain insight into the overall organization of these unusual structures, we reconstructed by means of STEM-HAAD tomography a large portion of a transfected HeLa cell (see supplementary material Movie 1 for a visualization of the entire tomogram, collected from three, 300nm-thick, plastic serial sections). As shown in Fig. 1C (in which mainly the cytosolic electron-dense layer is represented) and in supplementary material Movie 2 (in which the limiting cisternal membranes are shown), the structures

consist of a continuous ribbon of two to three parallel cisternae that follow a tortuous and sometimes convoluted pathway with frequent U-shaped turns.

In our previous work (Fasana et al., 2010), we generated HeLa-TetOff cell lines inducibly expressing a Myc-tagged version of P56S-VAPB, and showed at the light microscope level that the mutant protein, even when expressed at levels comparable to those of the endogenous protein, generated inclusions. To confirm that the structures visualized by immunofluorescence indeed correspond to the reorganized ER seen in transiently transfected cells, we analyzed the P56S-VAPB HeLa-TetOff cells by TEM, after either full [culture in the absence of doxycycline (Dox)] or intermediate induction (culture in the presence of low – 0.1 ng/ml – concentrations of the antibiotic). Under the latter condition, the levels of P56S-VAPB are similar to those of the endogenous, wild-type (wt) protein (Fasana et al., 2010). Under both conditions, structures identical to those seen in transiently transfected cells were readily detected (Fig. 1D–G), although, as expected, in the cells expressing low levels of the mutant protein, the restructured ER domains were less extended than in the fully induced or transiently transfected cells.

Aggregated P56S-VAPB is cleared from cells more rapidly than the wild-type protein

To investigate the fate of P56S-VAPB inclusions, we took advantage of the HeLa-TetOff system. Cells were first allowed to accumulate the mutant protein for 5–6 days in the absence of Dox; then, to stop synthesis of VAPB, the antibiotic was reintroduced into the medium, and the levels of Myc-tagged protein were subsequently analyzed during this chase period (Fig. 2A). To compare the degradation of the mutant with the wt protein, we generated HeLa-TetOff cell lines inducibly expressing wt Myc-tagged VAPB. As shown in supplementary material Fig. S1, the addition of Dox efficiently repressed expression of the transgene (panel A). After removal of the antibiotic, immunofluorescence analysis revealed that the wt protein localized to a normally branching ER, extending from the nuclear envelope to the cell periphery (panel B).

We first investigated the rate of decay of VAPB mRNA by RT-qPCR in the wt- and P56S-VAPB HeLa TetOff cells subjected to the 'pulse-chase' protocol illustrated in Fig. 2A. As shown in Fig. 2B, 6 h after re-introduction of Dox into the medium, VAPB mRNA levels were reduced by over 80% in both cell lines, with a further small reduction over the next four hours. We then analyzed the decay of the two proteins by immunoblotting. In these experiments, equal numbers of cells were seeded into wells two days before re-introduction of Dox. At each time point, equal aliquots of the entire cell population of one well were analyzed. By this procedure, dilution of VAPB (cell proliferation in the absence of VAPB synthesis) did not contribute to our analysis, as would have been the case if equal amounts of protein had been loaded in the lanes. These experiments showed an initial lag in the clearance of the two proteins, presumably due to translation of residual mRNA at the early time points of the analysis. At later time points (from 6 h on), the analysis revealed that P56S-VAPB is removed from the cells more rapidly than the wt protein (Fig. 2C,D): the level of mutant protein was reduced to ~50% at 7 h after Dox addition, compared to the ~17 h required for wt-VAPB to be similarly reduced.
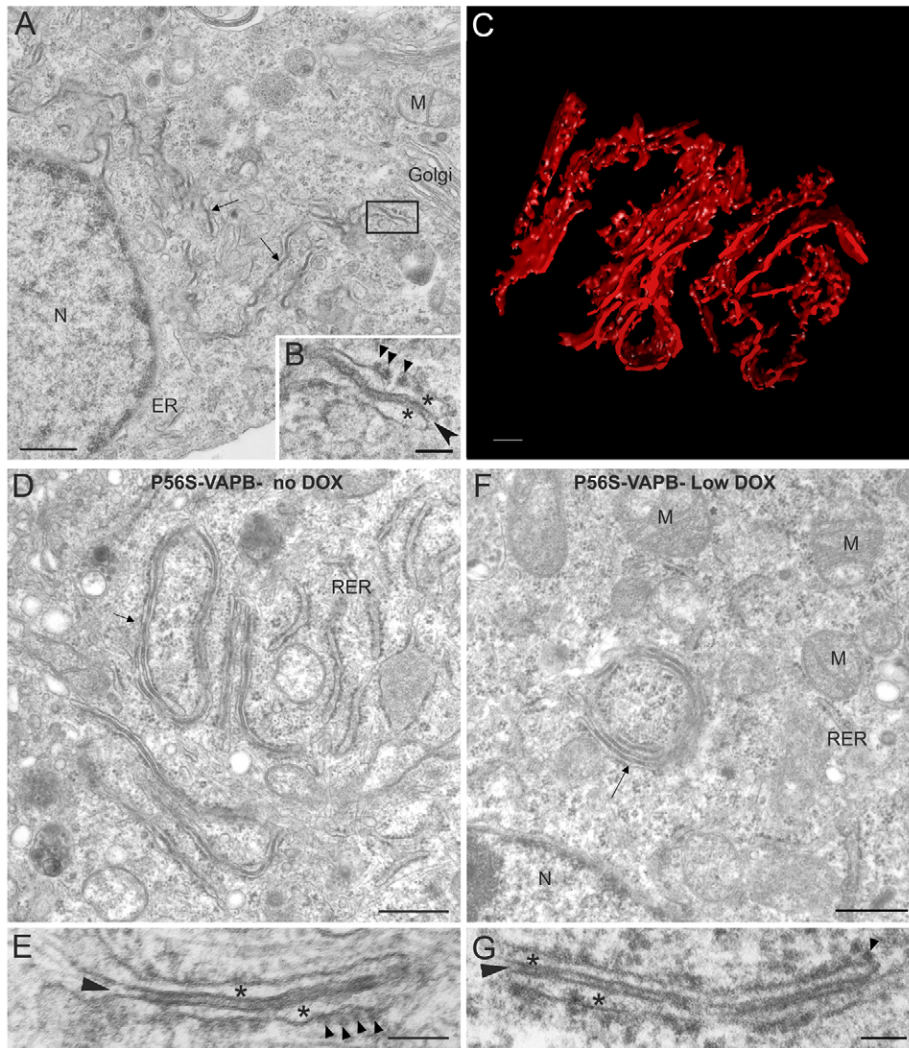
Fig. 1. Ultrastructure of P56S inclusions in transiently transfected and stably expressing HeLa cell lines. (A) Transient expression of P56S-VAPB induces the formation of convoluted electron-dense structures (arrows) in the perinuclear region. (B) Higher magnification of the boxed area in A. The altered ER typically consists of pairs of ER cisternae, interleaved by an electron-dense layer of cytosol. The continuity between this layer and the rest of the cytosol is indicated by the large arrowhead. Occasionally the cisternae of the altered ER are decorated by ribosomes (small arrowheads). The cisternal lumena are indicated by asterisks. (C) P56S-VAPB inclusions in a transiently transfected HeLa cell analyzed by STEM-HAAD tomography. A 3D reconstruction was obtained from a portion of the whole tomogram (boxed in supplementary material Movie 1). Automatic segmentation by a K-means clustering algorithm detected mainly the cytosolic dense layer. Membranes were nearly always invisible with these settings; however, the reconstruction permits visualization of the overall organization of P56S-VAPB inclusions. The 3D reconstruction confirms the presence of ER cisternae rather than tubules in the structures (see supplementary material Movies 1 and 2). (D–G) Ultrastructure of P56S-VAPB inclusions in an inducible HeLa-TetOff cell line after full induction by removal of Dox (D, E) or after partial induction by growth at low Dox concentrations (0.1 ng/ml; F,G). E and G show the details of the paired cisternae. The inclusions in the stable cell lines have the same structure as seen in transiently transfected cells. Large and small arrowheads and asterisks are as in A and B. Scale bars: 500 nm (A,D,F), 100 nm (B,E,G), 200 nm (C). M, mitochondrion; N, nucleus; RER, rough endoplasmic reticulum.

We then analyzed whether P56S remains in the inclusions during the chase period. As shown in Fig. 3A, P56S-VAPB was visualized within inclusions at times as long as 10 h after Dox re-addition, when most of the mutant protein has already been degraded (Fig. 2C,D). At this time, fewer cells had detectable P56S-VAPB inclusions, as expected (21 vs 26% at T_{10} and T_0,
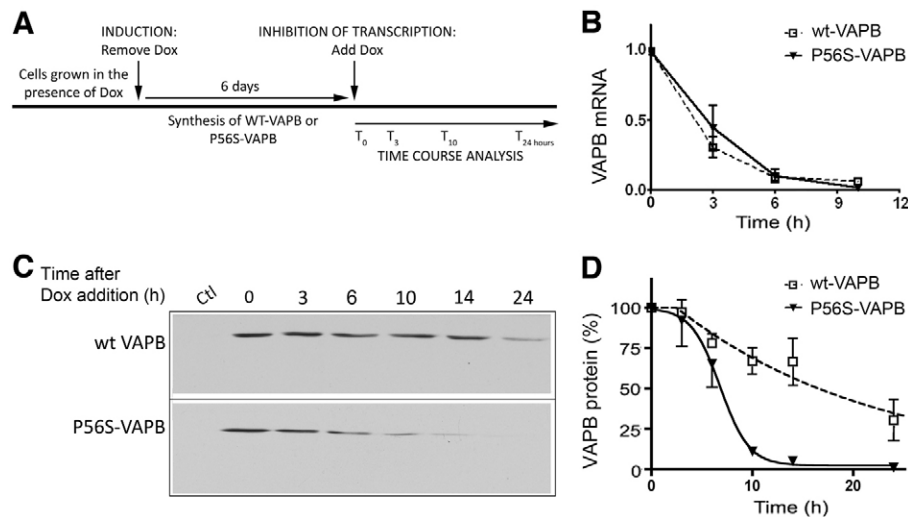
Fig. 2. Degradation of wt VAPB and P56S-VAPB. (A) Schematic representation of chase protocol adopted to investigate VAPB degradation. (B) Time course of wt VAPB and P56S-VAPB mRNA depletion from HeLa-TetOff cells after re-introduction of Dox. Values are normalized to GAPDH mRNA and expressed relative to T_0. Shown are the means ± half-range of two separate experiments, in each of which determinations were performed in triplicate. (C) Degradation of wt VAPB and P56S-VAPB assessed by immunoblotting with anti-Myc antibodies. Ctl, cells grown continuously in the presence of Dox. (D) Quantitative analysis of immunoblots such as that in C. In each experiment, optical density values of the bands were normalized to T_0. Each point represents the average of at least three separate experiments ± s.e.m.
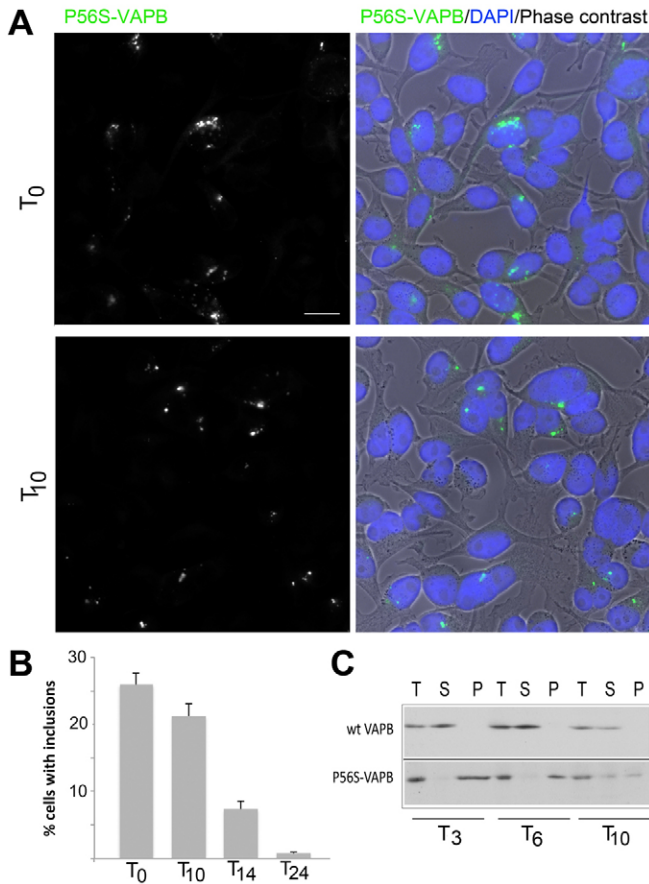
Fig. 3. P56S-VAPB remains in inclusions after cessation of its synthesis.
(A) Immunofluorescence analysis of P56S-VAPB in induced cells at the start
of the time course and 10 h after addition of Dox, as indicated. The images are
representative of 20 similar ones taken at random with a wide-field
microscope. The right column shows the superposition of the phase contrast
and DAPI stain with the Myc immunofluorescence. Scale bar: 10 µm.
(B) Time course of inclusion clearance after Dox addition to the medium. The
mean proportion of cells expressing detectable VAPB inclusions in 20
randomly acquired fields for each time point was determined. Bars represent
the s.e.m. (C) Analysis of the Triton X-100 solubility of wt and P56S-VAPB.
At the indicated times after Dox addition, cells were lysed in cold solution
containing Triton X-100. The lysates were separated into pellet and
supernatant fractions, and equal volumes of total lysate (T), pellet (P),
and supernatant (S) fractions were analyzed by immunoblotting with
anti-Myc antibodies.

respectively, Fig. 3B). At later time points, the proportion of
inclusion-bearing cells further decreased, until essentially
complete depletion at 24 h of chase (Fig. 3B).

The state of aggregation of mutant VAPB in comparison with
the wt protein was also assessed with a biochemical assay,
determining the solubility of the two proteins in Triton X-100
after cell lysis. Remarkably, whereas wt VAPB was recovered
only in the Triton-soluble fraction, P56S-VAPB remained largely
Triton-insoluble as long as it could be detected (Fig. 3C). A
higher proportion of mutant protein was solubilized in the 10 h
sample than at earlier time points, possibly because of the lower
concentration of the protein in cell lysates and the smaller size of
the inclusions at this time. Taken together, the biochemical and
the immunofluorescence data indicate that degradation of P56S-
VAPB is not preceded by bulk dissolution of the inclusions.

P56S-VAPB is polyubiquitinated and degraded by the proteasome

In the *Drosophila* model, mutant VAP inclusions are stained by anti-
ubiquitin (Ub) antibodies (Ratnaparkhi et al., 2008), and biochemical
assays have demonstrated that P56S-VAPB is polyubiquitinated
(Tsuda et al., 2008). In mammalian cells, mutant VAPB was found to
be conjugated to overexpressed HA-tagged Ub (Kanekura et al.,
2006), however, by immunofluorescence analysis Ub accumulation
in P56S-VAPB inclusions was weak or absent (Chen et al., 2010;
Teuling et al., 2007; Tudor et al., 2010). To clarify this discrepancy,
we carried out immunofluorescence analysis with anti-polyUb
antibodies on induced P56S-VAPB HeLa-TetOff cells. Co-
localization of polyUb with the inclusions was apparent (Fig. 4A),
although the intensity of polyUb staining was quite variable
(compare upper and middle rows of Fig. 4A), perhaps explaining
the differences in published results. Inclusions remained positive for
polyUb also 10 h after Dox removal (Fig. 4A, lower row).
Specificity of the labeling was confirmed by the absence of signal
on VAPB-positive inclusions when anti-polyUb primary antibody
was omitted from the immunostaining reactions (supplementary
material Fig. S2).

To confirm that mutant VAPB is linked to endogenous Ub, we
analyzed anti-Ub immunoprecipitates. Lysates prepared from
induced cells (T_0) or induced cells 10 h after re-addition of Dox
(T_{10}) were subjected to immunoprecipitation with anti-Ub
antibodies, and the resulting immunoprecipitates were analyzed
by immunoblotting with anti-Myc antibodies to detect P56S-
VAPB-Ub conjugates (Fig. 4B). Several Myc-positive bands,
which were absent in control samples (lanes 4, 6, and 8), were
detected in the anti-Ub immunoprecipitates from both T_0 and T_{10}
cells (lanes 5 and 7), confirming that P56S-VAPB becomes
ubiquitinated. In both the T_0 and T_{10} samples, some non-
ubiquitinated P56S-VAPB co-precipitated with the higher M_r
species. This observation suggests association between the
ubiquitinated and non-ubiquitinated forms, although we cannot
exclude that some deubiquitination of VAPB occurred during
preparation of the immunoprecipitates for SDS-PAGE.

To follow the timing of P56S-VAPB ubiquitination, we
adopted a cDNA microinjection protocol previously used to
analyze the time course of P56S-VAPB inclusion formation
(Fasana et al., 2010). In accordance with our previous
observations, as soon as mutant VAPB became detectable (2 h
after microinjection of the corresponding cDNA) it appeared
in dispersed small clusters, which later congregated in the
juxtanuclear region (Fig. 5A). At 2 and 4 h after microinjection,
Ub showed a dispersed punctate pattern, however, close
inspection of the cells revealed that even the small P56S-
VAPB clusters were positive for polyUb (see insets). At 6 h after
microinjection, polyUb concentration on the large juxtanuclear
inclusions was much easier to detect. However, quantitative
analysis showed that the ratio of polyUb to P56S-VAPB staining
remained constant over the entire time course (the values of this
ratio are indicated below the merged images of Fig. 5A),
indicating that ubiquitination of P56S-VAPB occurs rapidly
after its synthesis, and does not increase once clusters have
formed. To confirm this interpretation, we stopped protein
synthesis with cycloheximide at 6 h after microinjection, and
fixed the cells 3 h thereafter. The ratio of polyUb to P56S-VAPB
staining actually decreased after this treatment (fourth column of
Fig. 5A), in agreement with the hypothesis that P56S-VAPB
clusters/inclusions are not accessible to ubiquitin ligases.
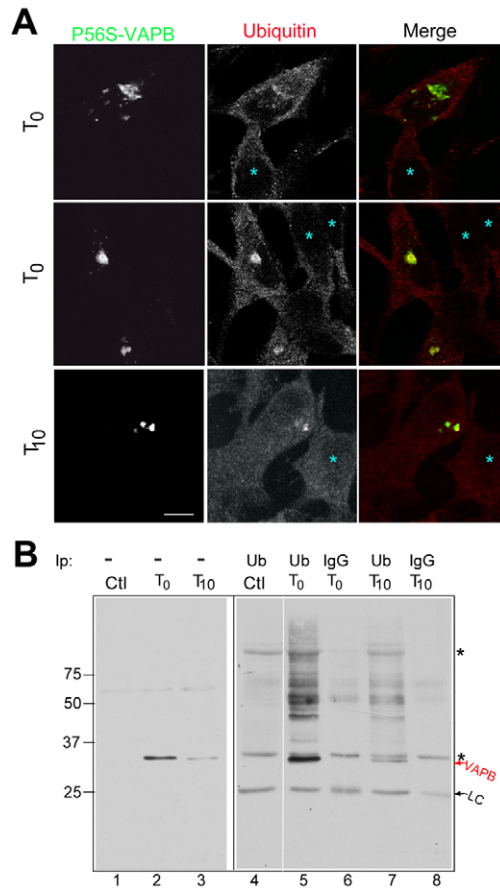
Fig. 4. Polyubiquitination of P56S-VAPB. (**A**) Double immunostaining of induced P56S-VAPB-HeLa-TetOff cells with anti-polyUb (red) and anti-VAPB (green) antibodies. The panel illustrates the variability in the intensity of polyUb staining, which is sometimes difficult to detect (top row), and in other cases quite pronounced (middle row). Inclusions remain positive for polyUb also at 10 h after Dox removal (bottom row). The cyan asterisks in the Ubiquitin and merge columns indicate cells with undetectable P56S-VAPB expression. (**B**) Immunoblotting analysis of anti-Ub immunoprecipitates. Lanes 1–3: total membrane fractions obtained from induced (T_0) cells, from an equal aliquot of induced cells 10 h after Dox re-addition (T_{10}), or from an equal aliquot of non-induced cells (Ctl), were analyzed by immunoblotting with anti-Myc antibodies. Lanes 4–8: the same membrane fractions (20 times the amounts analyzed in lanes 1–3) were subjected to immunoprecipitation with anti-Ub antibodies or non-specific IgGs, as indicated, and then analyzed by immunoblotting with anti-Myc antibodies. Lanes 1–3 and 4–8 are from different blots that were not exposed together, so the absolute intensities are not comparable between these two groups. Lanes 4–8 are from the same blot, and were all developed and exposed together. The asterisks indicate non-specific bands. LC, IgG light chain. Numbers on the left indicate the position and M_r ($\times10^{-3}$) of size markers. Scale bar: 10 μm.

The congregation of peripheral clusters of ubiquitinated mutant proteins is characteristic of a particular type of IB, known as aggresome (Kopito, 2000). Aggresomes are formed by transport of peripheral clusters of malfolded ubiquitinated proteins along microtubule tracks to a juxtanuclear region in the vicinity of the microtubule organizing centre. To investigate whether microtubules are involved also in the transport of P56S-VAPB clusters from the periphery to the cell centre, we followed the generation of inclusions in microinjected cells after disruption of the microtubule cytoskeleton by nocodazole. Again, dispersed

clusters were seen as soon as the protein was detectable (Fig. 5B, left panel), and concentration in a large juxtanuclear structure was complete in most cells at 6 h after the microinjection (Fig. 5B, third panel), in a manner indistinguishable from that of untreated cells (Fig. 5B, right panel). This result reveals an important mechanistic difference between the genesis of classical aggresomes and of P56S-VAPB inclusions.

In recent years it has become apparent that Ub serves as a signal for the delivery of proteins not only to the proteasome but also to the macroautophagosomal (autophagosomal) degradation pathway (Bjorkoy et al., 2005; Kirkin et al., 2009). We therefore investigated the contribution of the proteasome and of autophagocytosis to P56S-VAPB elimination by the use of specific inhibitors of each of these pathways. The proteasomal inhibitor MG-132 nearly completely blocked degradation of the mutant protein (Fig. 6A,B), with the consequent persistence of ubiquitinated inclusions (Fig. 6B,C). In contrast, treatment of the cells with the autophagocytosis inhibitor 3-Methyladenine (3-MA) had no effect on P56S-VAPB degradation (Fig. 6A,B), although it did inhibit starvation-induced autophagocytosis (supplementary material Fig. S3).

Wild-type VAPB is known to be sequestered within P56S-VAPB IBs, and this sequestration has been suggested to underlie the dominant inheritance of the mutant protein (Kanekura et al., 2006; Suzuki et al., 2009; Teuling et al., 2007). We asked whether the presence of P56S inclusions might accelerate the degradation of the sequestered, endogenous, wt protein. As shown in Fig. 6D, expression of neither wt nor P56S-VAPB had any effect on the steady state levels of the endogenous protein (which has a higher mobility in SDS-PAGE than the Myc-tagged wt and mutant proteins). This result is consistent with the notion that P56S-VAPB degradation proceeds molecule by molecule, and is instead difficult to reconcile with a bulk elimination process mediated by autophagy.

To further investigate the relationship between P56S-VAPB inclusions and autophagocytosis, we compared the distributions of mutant VAPB and the autophagosomal, Ub binding protein p62 (also known as sequestosome) (Bjorkoy et al., 2005; Komatsu et al., 2007; Pankiv et al., 2007). In striking contrast with the observations on IBs that characterize other neurodegenerative diseases (Kuusisto et al., 2001; Nagaoka et al., 2004; Zatloukal et al., 2002), we detected no colocalization between mutant VAPB inclusions and p62 (Fig. 6E, upper row). We also analyzed cells in which autophagy was induced by serum starvation (Fig. 6E, lower row). As expected, starvation caused a reduction in the overall intensity of p62 staining, consistent with its enhanced degradation in this condition (Bjorkoy et al., 2005; Komatsu et al., 2007), while p62-positive puncta, corresponding to autophagosomes/autolysosomes, became more apparent. Also in these serum-starved cells, we found no co-localization between VAPB and p62, although, quite strikingly, p62-positive structures were often closely juxtaposed to the VAPB inclusions. Similar results were obtained with the autophagosomal marker LC3 (Kabeya et al., 2000) (supplementary material Fig. S4).

The 43 kDa TAR DNA-binding protein (TDP-43) has been found as a major component of ubiquitinated, p62-positive, protein aggregates in ALS patients (Ince et al., 2011). We therefore investigated whether such aggregates are present in our induced cells, and, if so, whether they coincide with the P56S-VAPB inclusions. Our analysis failed to reveal any dislocation of
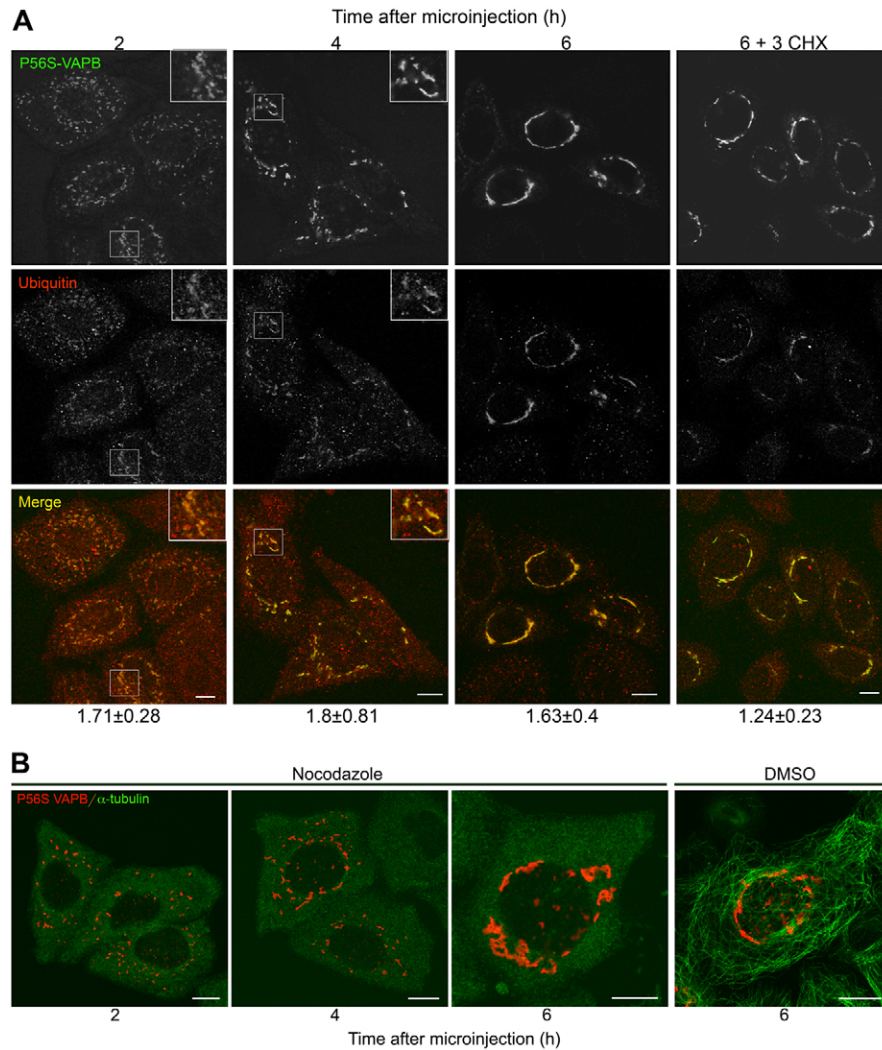
Fig. 5. Analysis of the generation of P56S-VAPB inclusions in microinjected cells. (**A**) P56S-VAPB clusters are positive for polyUb as soon as they become detectable. HeLa cells were microinjected with a cDNA coding for P56S-VAPB under the CMV promoter. At the indicated times after microinjection, cells were fixed and doubly immunostained for polyUb (red) and VAPB (green). Images were acquired with identical parameters and slightly contrasted with Adobe Photoshop together. The samples shown in the right column were treated with cycloheximide at 6 h after microinjection, and fixed 3 h thereafter. The numbers below the merged images indicate the ratio of polyUb to VAPB staining intensities ± s.d. (10 fields, containing 2–3 cells for each determination). (**B**) Microtubule integrity is not required for the clustering of P56S-VAPB inclusions in the juxtanuclear region. Cells were microinjected as in A and then immediately transferred to medium containing nocodazole or an equal volume of the vector (DMSO). Cells were fixed at the indicated times. Congregation of the peripheral P56S-VAPB clusters at the juxtanuclear region proceeds undisturbed in the nocodazole-treated cells. Scale bars: 10 μm; insets are magnified twofold.

TDP-43 from its normal nuclear localization to cytoplasmic inclusions (supplementary material Fig. S5, top row). Instead, similar to our observations on transiently transfected cells (Fasana et al., 2010), we observed accumulation in the inclusions of Bap31, an ER protein that has been implicated in chaperoning ER membrane proteins to ERAD (Wakana et al., 2008) (supplementary material Fig. S5, bottom row).

Role of the AAA-ATPase p97/VCP in the delivery of P56S-VAPB to the proteasome

Since VAPB is an ER transmembrane (tail-anchored) protein, and the inclusions that it generates consist of restructured ER domains, we reasoned that its delivery to the proteasome must involve extraction not only from the aggregates, but also from the ER membrane. We therefore investigated a possible involvement of the AAA chaperone, p97 (also known as valosin-containing protein, VCP), an ATPase that extracts ERAD substrates from the ER to deliver them to the proteasome (Rabinovich et al., 2002; Ye et al., 2001). To analyze the role of p97/VCP in P56S-VAPB degradation, induced P56S-VAPB TetOff cells were transfected with cDNAs coding either for the wt or a mutant (QQ), ATPase-deficient, p97 (Ye et al., 2001). The QQ mutant has been shown to act as a dominant negative (DN), thereby inhibiting substrate

extraction from the ER (Ye et al., 2001). As shown in Fig. 7, in cells transfected with wt-p97, P56S-VAPB was degraded with the same time course as in the non-transfected cells. In contrast, transfected DNp97 stabilized the mutant protein, more than doubling its concentration at T_{10} relative to T_0 in comparison to the control cells.

Discussion
Unique features of P56S-VAPB inclusions
Since its discovery (Nishimura et al., 2004), FALS-linked P56S-VAPB was observed to form inclusions in cultured cells that appeared similar to those generated by mutant proteins underlying other neurodegenerative diseases such as polyQ expanded Huntingtin in Huntington's disease, mutated synuclein in Parkinson's disease, and neurofibrillary tangles in Alzheimer's disease (Ross and Poirier, 2004). Further investigations, however, revealed important differences between P56S-VAPB inclusions and other IBs. More specifically, mutant VAPB inclusions correspond to a profoundly restructured ER domain and not to a cytosolic protein aggregate, as is the case for most IBs. Our previous work (Fasana et al., 2010) demonstrated that P56S-VAPB, like the wt protein, inserts into the ER membrane via its C-terminal tail, but that after insertion it rapidly
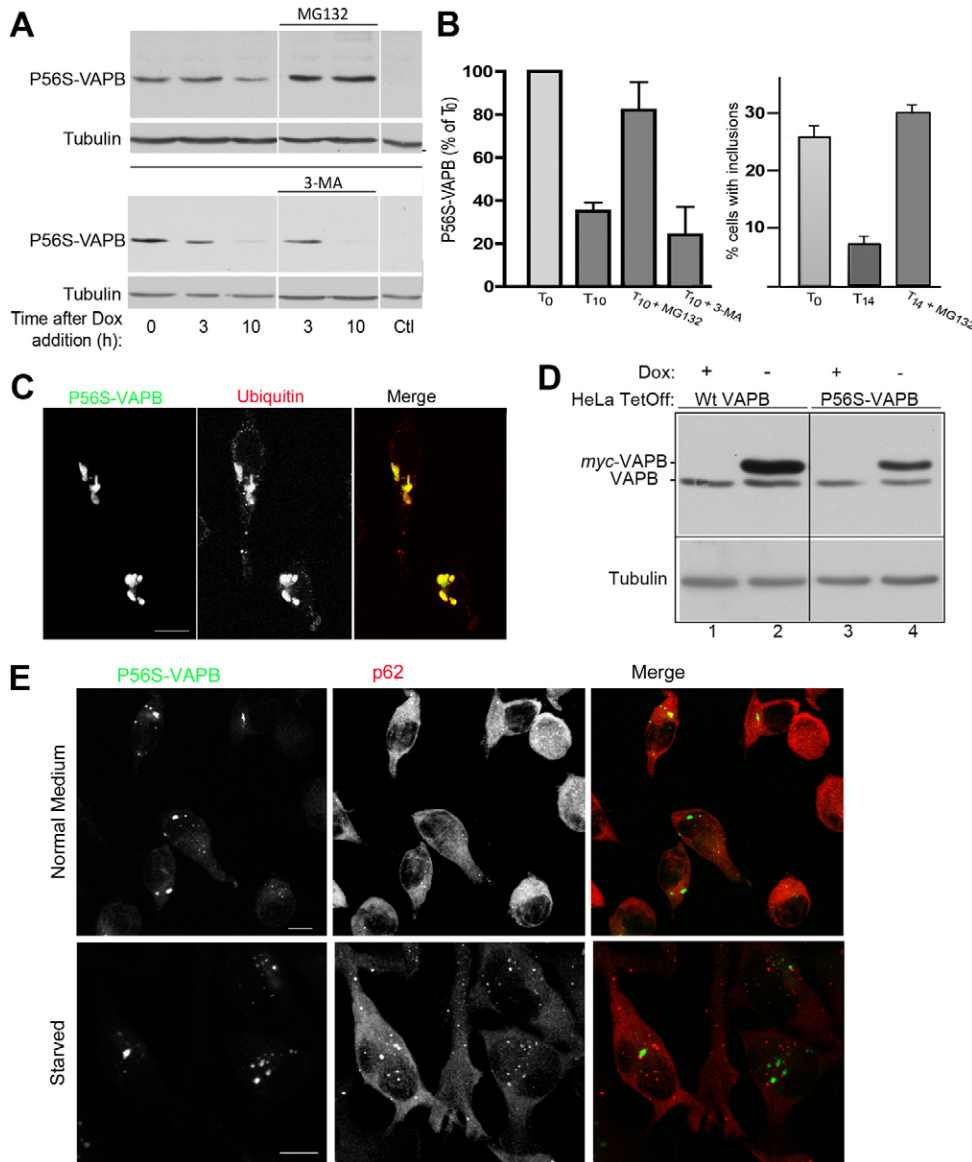
Fig. 6. P56S-VAPB inclusions are cleared by the proteasome. (**A**) Immunoblotting analysis of P56S-VAPB degradation in the presence of a proteasomal (MG-132) or autophagocytosis (3-MA) inhibitor. The experiment was carried out as in Fig. 2, but 3 h after the addition of Dox, the inhibitors were added, where indicated. Ctl, cells grown continuously in the presence of Dox. Each set of six lanes of the upper and lower panel are from the same blot. (**B**) Left graph shows quantitative analysis of data illustrated in A. In each experiment, optical density values of the bands were normalized to that at T_0. Each point represents the average of two biological replicates ± half-range. Graph on right shows that MG-132 inhibits inclusion clearance. The mean proportion of cells expressing detectable VAPB inclusions in 20 randomly acquired fields for each time condition is shown. Bars indicate the s.e.m. (**C**) Double immunostaining of T_{10} cells exposed to MG-132 after addition of Dox reveals large P56S-VAPB inclusions positive for polyUb. (**D**) The levels of endogenous wt VAPB are not altered by the expression of the mutant protein. Immunoblot analysis of lysates from wt or P56S-VAPB HeLa-TetOff cells grown in the presence or absence of Dox, as indicated. The blot was probed with an anti-VAPB antibody, which recognizes both the endogenous and the Myc-tagged protein. (**E**) Lack of colocalization of p62 and P56S-VAPB inclusions. Induced HeLa-TetOff cells were exposed to Dox in complete medium for 3 h (top row). They were then shifted to serum-free medium in the presence of Dox for a further for 3 h (bottom row). The cells were fixed and doubly immunostained for VAPB (green) and p62 (red). Scale bars: 10 μm.

clusters, generating paired ER cisternae apparently held together by the interactions between the mutant cytosolic domains (Fasana et al., 2010). We classified these restructured ER domains as a particular form of organized smooth ER (OSER) (Snapp et al., 2003), which consists in different varieties of organized arrays of stacked smooth cisternae. Differently from previously described OSER, however, the stacks of P56S-VAPB inclusions do not form multi-layered arrays; rather, a limited number (two to three) of stacked cisternae form a ribbon that undergoes a convoluted, tortuous pathway, as confirmed here by tomographic analysis.

In the present study, we have uncovered additional interesting characteristics of P56S-VAPB inclusions that set them apart from other IBs. First, although the inclusions contain polyubiquitinated P56S-VAPB and are located in a juxtanuclear position, they do not require the microtubule cytoskeleton to attain this location; and, second, the inclusions are cleared rapidly by the proteasome by a process requiring the AAA ATPase p97. We discuss these two findings in turn.

The juxtanuclear localization of P56S-VAPB inclusions does not depend on the microtubule cytoskeleton

Microtubules, associated with negative end directed molecular motors, are involved in transport of cellular components from the periphery to the juxtanuclear region. In particular, the aggresome, a particular type of IB, is generated by transport of peripheral clusters of malfolded proteins along microtubule tracks (Kopito, 2000). The proteins in the peripheral clusters are usually polyubiquitinated, and the deacetylase HDAC6 serves as adaptor between ubiquitin and the dynein motor (Kawaguchi et al., 2003). Given the generality of these findings, we expected to find a role for microtubules in the congregation of P56S-VAPB inclusions. In contrast to the previously investigated protein inclusions, however, disruption of the microtubule cytoskeleton was without effect on the localization of the mutant protein. This negative result, while uncovering another difference between mutant VAPB inclusions and well characterized IBs linked to neurodegeneration, leaves the mechanism of congregation of
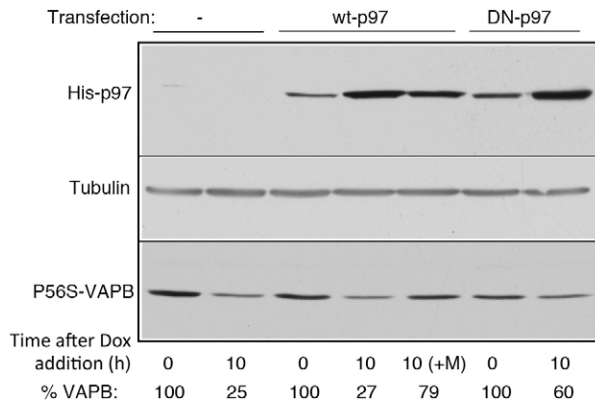
Fig. 7. Role of the AAA ATPase p97/VCP in P56S-VAPB degradation. Induced HeLa-TetOff cells were transfected either with wt or dominant-negative (DN) His-tagged p97 or with an equal amount of empty vector (first two lanes), as indicated. One day after the transfection, cells were collected, or incubated in the presence of Dox for a further 10 h. MG-132 was added to one sample 3 h after addition of Dox [fifth lane, indicated as 10(+M)]. Total lysates were analyzed by immunoblotting with anti-Myc (lower panel), anti-tubulin or RSG-His antibodies (to reveal p97). The numbers below the lanes, which indicate the percentage of VAPB at T_{10} versus T_0, are the average of two experiments.

P56S-VAPB inclusions unresolved. We note, however, that in cultured mammalian cells ER cisternae are enriched in the paranuclear region (Puhka et al., 2007), and suggest that simple geometrical constraints could favour entrapment of both normal, ribosome-covered cisternae and P56S-VAPB paired cisternae in the central, thicker and less dynamic portions of the cell.

After aggregation, P56S-VAPB is eliminated by the proteasome

The observation that P56S-VAPB is cleared from cells more rapidly than its wt counterpart was also unexpected. Indeed, although many mutant proteins are destabilized, large aggregates are thought to be thermodynamically stable (Fink, 1998). Even more surprising was the involvement of the proteasome and the lack of involvement of the autophagy pathway, as indicated by the near complete inhibition of P56S-VAPB degradation by the proteasomal inhibitor MG-132, by the lack of effect of the autophagy inhibitor 3-MA, and by the absence in the inclusions of LC3 and p62, a Ub receptor that is thought to mediate the selective autophagy of ubiquitinated protein aggregates (Kirkin et al., 2009; Komatsu et al., 2007; Pankiv et al., 2007). Our microinjection experiment demonstrated that mutant VAPB becomes polyubiquitinated shortly after its synthesis; nonetheless at least a part of the ubiquitinated protein initially avoids the proteasome, forming the restructured ER inclusions that are only subsequently cleared from the cell. Thus, the rapidity of the aggregation process may initially protect mutant VAPB from proteasomal attack.

A number of IBs are known to be cleared by autophagocytosis, including those formed by polyQ or polyA expanded proteins (Iwata et al., 2005; Ravikumar et al., 2002), and by synuclein (Olzmann and Chin, 2008; Webb et al., 2003). Autophagocytosis also plays a role in the elimination of inclusions generated by mutant cystic fibrosis transmembrane conductance regulator (CFTR) (Fu and Sztul, 2009), and of organized smooth ER (Lingwood et al., 2009). Thus, P56S-VAPB inclusions appear to

stand apart from other IBs, both in the mechanism of their genesis and of their clearance from the cell.

Delivery of unfolded/malfolded ER proteins to the proteasome involves a complex process known as ERAD (Bernasconi and Molinari, 2011). A keyplayer in ERAD is the AAA-ATPase p97/VCP, which utilizes ATP hydrolysis to pull substrates out of or across the ER membrane into the cytosol (Rabinovich et al., 2002; Ye et al., 2001). Our results with a dominant negative form of p97/VCP (QQ-p97) indicate that delivery of P56S-VAPB to the proteasome requires the activity of this ATPase; however, at present we do not know its exact role in the process. By fluorescence recovery after photobleaching (FRAP), P56S-VAPB appears to be immobilized within the inclusions that it generates (Teuling et al., 2007). Thus, p97/VCP may be required not only to pull the transmembrane domain out of the lipid bilayer but also to dissolve the protein-protein interactions underlying inclusion formation. We cannot, however, exclude that mutant VAPB molecules slowly exchange with the surrounding ER at a rate too low to be detected by the FRAP experiments of Teuling et al. (Teuling et al., 2007). In this case, p97/VCP would be acting as a trap, extracting single P56S-VAPB molecules from the bilayer as they gradually become available.

Relevance of our findings to the pathogenic mechanism of P56S-VAPB

Dominant inheritance, as is the case for the P56S-VAPB mutation, can be explained by gain of function (toxicity of the altered gene product) and/or loss of function (negative dominance, and/or haploinsufficiency) or by combinations of these mechanisms. It has recently been reported that overexpressed P56S-VAPB may exert a cytotoxic effect by inhibiting the proteasome (Moumen et al., 2011); however, in that study, the wild-type and mutant protein had similar effects. Thus, any toxic effect specifically attributable to P56S-VAPB inclusions remains to be demonstrated. Instead, the finding that wt VAPB (and to a lesser extent its homologue VAPA) is sequestered within mutant VAPB inclusions (Kanekura et al., 2006; Suzuki et al., 2009; Teuling et al., 2007), has favoured the hypothesis that negative dominance underlies the pathogenicity of P56S-VAPB. This hypothesis predicts that expression of the mutant protein in the background of a normal VAPB genotype should be sufficient to induce ALS pathology. In fly models, this prediction is borne out (Chai et al., 2008; Ratnaparkhi et al., 2008), however, the situation in mammals is less clear. While heavy overexpression of P56S-VAPB, but not of the wt protein, does increase cell death of primary neurons and neuronal cell lines (Suzuki and Matsuoka, 2011; Teuling et al., 2007), P56S-VAPB transgenic mice do not develop any motor deficit (Tudor et al., 2010). Furthermore, and importantly, a recent study failed to detect VAPB inclusions in motor neurons derived from induced pluripotent stem cells of patients carrying the P56S-VAPB mutation (ALS8 patients), but did reveal reduced levels of VAPB within these cells (Mitne-Neto et al., 2011). These findings are fully consistent with our results demonstrating the relatively rapid clearance of mutant P56S-VAPB inclusions.

On the basis of our results, and of the studies on transgenic mice (Tudor et al., 2010) and cells from human patients (Mitne-Neto et al., 2011), we suggest that haploinsufficiency may be the principal mechanism underlying P56S-VAPB pathogenicity. Of note, two studies have reported a reduction in VAP levels in spinal cord motor neurons of sporadic ALS patients and of

transgenic mice (G93A superoxide dismutase-1) with ALS pathology (Anagnostou et al., 2010; Teuling et al., 2007), suggesting that the reduction of VAPB levels, caused either by mutation or by other unknown causes, may play a general role in the pathogenesis of both the sporadic and the familial forms of ALS.

VAPB has been implicated in a variety of functions, among which interorganellar contacts and non-vesicular transport of lipids between the ER and other organelles (Kawano et al., 2006; Loewen and Levine, 2005; Peretti et al., 2008; Stefan et al., 2011), organelle-microtubule interactions (Amarilio et al., 2005; Rocha et al., 2009), neurite extension (Saita et al., 2009), vesicular trafficking (Foster et al., 2000; Skehel et al., 1995; Soussan et al., 1999), and the Unfolded Protein Response (Chen et al., 2010; Gkogkas et al., 2008; Kanekura et al., 2006; Suzuki et al., 2009). At present, one can only make educated guesses as to which of these processes is/are impaired in cells with reduced levels of VAPB. Identification of the VAPB functions that require homozygous levels of the protein to maintain motor neurons in good health will be an important milestone towards unravelling the factors underlying sporadic and familial ALS.

Materials and Methods
Plasmids
The pCAN-*myc*-P56S-VAPB plasmid, coding for Myc-tagged human P56S-VAPB and used for expression in transiently transfected and microinjected cells, has been described (Fasana et al., 2010). For inducible expression of wt VAPB in HeLa-TetOff cells, a cDNA fragment coding for Myc-VAPB (wt), a gift from Sima Lev (Weizmann Institute of Science, Rehovot, Israel) was subcloned into the pTre tight vector (Clontech). Plasmids pCDNA3-His-p97 (wt and dominant negative QQ mutant) and pGFP-LC3 (Kabeya et al., 2000) were gifts from Yinhong Ye (NIH/NIDDH) and Sharon Tooze (Cancer Research UK), respectively.

Antibodies
To visualize Myc-tagged VAPB by immunofluorescence or immunoblotting, we generally used anti-Myc monoclonals (clone 9E10 from Santa Cruz or Sigma). In some cases it was necessary to visualize VAPB with polyclonal antibodies; in these cases, we used either a polyclonal anti-Myc (from Cell Signaling) or an anti-VAPB antibody donated by Casper C. Hoogenraad (Utrecht University). Anti-polyUb (clone FK1) and anti-mono and polyUb (clone FK2), used for immunofluorescence and for immunoprecipitation, respectively, were from BioMol. Anti-TDP43 and anti-tubulin polyclonals were from Sigma. Anti-HA was from Santa Cruz, and anti-p62 was obtained from AbCam. RSG-His antibody was from Qiagen. An anti-Bap31 polyclonal was a gift from Mitsuo Tagaya (Tokyo University of Pharmacy and Life Sciences).

Alexa Fluor 488 and 568 secondary antibodies were from Invitrogen. Rhodamine-conjugated anti-mouse IgM antibodies were from Santa Cruz. Peroxidase-conjugated anti-rabbit and anti-mouse IgG were from Sigma, and light chain-specific anti-rabbit IgG was from Jackson ImmunoResearch.

Cell culture, transient transfection and microinjection
HeLa-TetOff clones expressing Myc-tagged wt VAPB were selected, maintained in culture and induced to express the transgene by growth in the absence of Dox for 5–6 days as previously described for the Myc-tagged P56S-VAPB clones (Fasana et al., 2010). For both the wt and the mutant VAPB two separate clones were used, with similar results. Transfection of P56S-VAPB TetOff cells with the indicated plasmids was carried out by the $CaPO_4$ method 24 h before harvesting or fixing the induced or non-induced cells.

Non-transfected HeLa cells were maintained in culture and microinjected or transfected with pCAN-*myc*-P56S-VAPB, as previously described (Fasana et al., 2010).

Time course of VAPB degradation
Equal numbers (~400,000) of Myc-tagged-wt or P56S-VAPB (referred to simply as wt or P56S-VAPB) HeLa TetOff cells, grown for 4 days in the absence of Dox, were seeded in 60 mm Petri dishes, each containing a coverslip. After 48 h in the absence of the Dox, the coverslips were removed and stained with DAPI; the DAPI-stained nuclei were counted in order to check that each dish contained the same number of cells. Cells from the dish corresponding to the first time point (T_0) were collected and lysed with 0.5 ml pre-warmed (80°C) lysis buffer [2% SDS, 50 mM Tris-HCl, pH 8, plus Complete (Roche) protease inhibitors]. The other

dishes were supplemented with Dox (0.5 µg/ml) and returned to the incubator; cells were harvested at the indicated time points with the same volume of lysis buffer as the T_0 cells. Equal volumes of the lysates were analyzed by SDS-PAGE-immunoblotting.

SDS-PAGE immunoblotting
SDS-PAGE and blotting were carried out by standard procedures. Blots were incubated with primary antibodies diluted in Tris-saline, 5% milk, 0.1% Tween, unless alternative conditions were recommended by the supplier. After incubation with peroxidase-conjugated secondary antibodies, the blots were developed with ECL-Plus or ECL-Ultra (GE Healthcare) reagents. The films were digitized, and band intensities were determined with ImageJ software (National Institutes of Health) after calibration with the optical density calibration step table (Stouffer Graphics Arts).

Immunoprecipitation
Cells grown to 80% confluence in two 10 mm Petri dish were harvested and resuspended in 0.6 ml of a hypotonic solution, containing 1 mM Tris-HCl, pH 7.4, 15 mM KCl, 0.1 mM EDTA, Complete (Roche) protease inhibitors, and incubated on ice for 5 min. After homogenizing the samples by repeated passages through an insulin syringe, an equal volume of a solution containing 2 mM Tris-HCl, pH 7.4, 0.5 M sucrose, 0.2 mM EDTA, and protease inhibitors was added to restore isotonicity. The samples were centrifuged at 200,000 *g* at 4°C for 1 h, and the supernatant, containing cytosolic proteins, was discarded. The pellets were lysed with 1 ml of a pre-warmed buffer (80°C) containing 1% SDS, 50 mM Tris-HCl, pH 8, plus protease inhibitors. After shearing the released DNA by repeated freeze-thawing and passage through an insulin syringe, nine volumes of a buffer containing 0.140 M NaCl, 50 mM Tris-HCl, pH 7.5, 5 mM EDTA, pH 8, 2.2% Triton X-100 was added. After removing any insoluble material by centrifugation at 12,000 *g* for 10 min, a small aliquot of the sample was kept to analyze the input, while the rest was subjected to immunoprecipitation with anti-Ub monoclonals or unrelated mouse IgGs. Immunocomplexes were collected with agarose-Protein G beads and analyzed by immunoblotting with anti-Myc polyclonal antibodies.

Triton X-100 solubility assay
All solutions contained Complete (Roche) protease inhibitors. Cells grown to 80% confluence on 60 mm plates were harvested and resuspended with 0.25 ml of a solution containing 10 mM Tris-HCl, pH 7.4, 1 mM EDTA. The samples were then lysed with an equal volume of 2% Triton X-100 in the same Tris-EDTA buffer. After 30 min on ice, 100 µl were removed for the analysis of the total sample, and the remaining lysates were centrifuged at 12,000 *g* for 10 min. After withdrawal of the supernatants, the pellets were resuspended in 200 µl of 10 mM Tris-HCl, pH 7.4, and treated with DNase (40 µg/ml final concentration) to digest any released DNA. The resuspended pellets were then brought to 400 µl, and equal aliquots of the total samples, pellets and supernatants were analyzed by SDS-PAGE/immunoblotting.

RT-qPCR
Total RNA was extracted using the RNeasy Mini Kit and accompanying QIAshredder (Qiagen) according to the manufacturer's instructions. Contaminating DNA in the sample was degraded by on-column incubation with DNaseI (Qiagen) for 15 min. 1 µg per sample was reverse-transcribed using the SuperScript III First- Strand Synthesis System for RT-PCR (Invitrogen) in accordance with the manufacturer's instructions. P56S-VAPB mRNA levels were quantitatively analyzed by the SYBR green method, with forward primer (specific for the Myc-tagged sequence) 5′-AGCTGATCTCCGAGGAGGACCTG-3′, and reverse primer 5′-TTTCGGTCTGTCGGGTTGCC-3′. The size of the PCR products was confirmed by gel electrophoresis. Amplification was carried out with the ABI Prism 7000 Sequence Detection System and SDS software version 1.2.3 (Applied Biosystems). The cycling conditions were one cycle of denaturation at 95°C for 10 min, followed by 40 two-segment cycles of amplification (95°C for 15 s and 60°C for 1 min). At the end of the cycles, a dissociation protocol (95°C for 15 s, 60°C for 20 s, and 95°C for 15 s) was run to verify the presence of one gene-specific peak and the absence of primer-dimers. All samples were amplified in triplicate. The $2^{-\Delta\Delta CT}$ method was used to calculate the results, which were normalized to GAPDH mRNA, used as internal control (forward primer, 5′-TCG-GAGTCAACGGATTTGG-3′, reverse primer, 5′-TGGCAACAATATCCACT-TTACCA-3′; Gen-Bank accession no. NM_002046.3).

Drug treatment
3-MA, dissolved in water, was used at a final concentration of 10 mM. Cycloheximide was dissolved in PBS and used at a final concentration of 50 µg/ml. Nocodazole and MG-132 were dissolved in DMSO and used at final concentrations of 3 and 10 µg/ml respectively. Control cells received equal volumes of the vector.

Immunofluorescence

Cells grown on coverslips were fixed with 4% paraformaldehyde and processed for immunofluorescence, as described previously, with minor modifications (Fasana et al., 2010), using Alexa- or Rhodamine-conjugated secondary antibodies (Invitrogen). To visualize GFP-LC3 together with P56S-VAPB, paraformaldehyde-fixed cells were permeabilized with methanol instead of Triton, and antibodies were diluted in PBS + 0.1% bovine serum albumin. Cells were imaged with the Zeiss LSM 510 Meta confocal system (Carl Zeiss, Oberkochen, Germany) using a 63× PlanApo lens. Alexa Fluor 488 and GFP were imaged with the use of the 488 line of the Argon/2 laser, a 405/488/543/633 dichroic, and a 505–550 band pass emission filter. For Alexa 568 and Rhodamine, the 544 line of the He/Ne laser was used, with the same dichroic as above, and a 560 longpass emission filter. Wide-field imaging was performed with an Axioplan microscope (Carl Zeiss, Oberkochen, Germany), using the 40× PlanNeofluar lens equipped with a phase contrast ring. Illustrations were prepared with Adobe Photoshop software.

To determine the ratio of polyUb to P56S-VAPB staining, series of images (10 for each condition) were acquired all with identical parameters, taking care to remain below saturation in both the Ub (Alexa 568) and the VAPB (Alexa 488) channels. Each image was segmented in the VAPB channel, and a mask corresponding to VAPB staining was used to determine the mean grey value in both channels with the use of ImageJ software.

Electron microscopy

Cells were fixed as a monolayer in 2% glutaraldehyde, 0.1 M cacodylate buffer for 30 min at room temperature and further processed for transmission EM as previously described (Fasana et al., 2010; Snapp et al., 2003). Epon thin sections were observed with a Philips CM10 transmission electron microscope (Philips, Amsterdam, The Netherlands) equipped with a Morada EM CCD-camera (from Olympus SIS). Digital images were acquired using the iTEM software (from Olympus-SIS).

STEM-HAAD (High-Angular Annular Dark-Field) tomography was performed with a JEOL JEM 2200 FS EM operating at 200 kV, using a spot size of 1 nm and the smallest condenser aperture resulting in a collection angle of 3 mrad. The sample (300 nm thick serial sections) was mounted on a Fischione Ultra-Narrow Gap Tomography Holder and tilted over a ± 60 range every 2 degrees or according to a 'Saxton scheme'. Images were acquired using a HAADF detector at a magnification of 40,000×, resulting in a pixel resolution of 7.93 nm.

Serial section tomograms were reconstructed and joined using the IMOD software package (Kremer et al., 1996; Mastronarde, 1997). A tomogram sub-volume was automatically segmented using a K-means clustering algorithm implemented with MATLAB. The binary output was Gaussian filtered to reduce noise and rendered using UCSF Chimera package. Alternatively, selected structures of the tomogram were rendered by manual segmentation using IMOD.

Supplementary material available online at
http://jcs.biologists.org/lookup/suppl/doi:10.1242/jcs.102137/-/DC1

References

Amarilio, R., Ramachandran, S., Sabanay, H. and Lev, S. (2005). Differential regulation of endoplasmic reticulum structure through VAP-Nir protein interaction. *J. Biol. Chem.* **280**, 5934-5944.

Anagnostou, G., Akbar, M. T., Paul, P., Angelinetta, C., Steiner, T. J. and de Belleroche, J. (2010). Vesicle associated membrane protein B (VAPB) is decreased in ALS spinal cord. *Neurobiol. Aging* **31**, 969-985.

Andersen, P. M. and Al-Chalabi, A. (2011). Clinical genetics of amyotrophic lateral sclerosis: what do we really know? *Nat Rev Neurol* **7**, 603-615.

Arrasate, M., Mitra, S., Schweitzer, E. S., Segal, M. R. and Finkbeiner, S. (2004). Inclusion body formation reduces levels of mutant huntingtin and the risk of neuronal death. *Nature* **431**, 805-810.

Balch, W. E., Morimoto, R. I., Dillin, A. and Kelly, J. W. (2008). Adapting proteostasis for disease intervention. *Science* **319**, 916-919.

Bence, N. F., Sampat, R. M. and Kopito, R. R. (2001). Impairment of the ubiquitin-proteasome system by protein aggregation. *Science* **292**, 1552-1555.

Bernasconi, R. and Molinari, M. (2011). ERAD and ERAD tuning: disposal of cargo and of ERAD regulators from the mammalian ER. *Curr. Opin. Cell Biol.* **23**, 176-183.

Bjørkøy, G., Lamark, T., Brech, A., Outzen, H., Perander, M., Overvatn, A., Stenmark, H. and Johansen, T. (2005). p62/SQSTM1 forms protein aggregates degraded by autophagy and has a protective effect on huntingtin-induced cell death. *J. Cell Biol.* **171**, 603-614.

Chai, A., Withers, J., Koh, Y. H., Parry, K., Bao, H., Zhang, B., Budnik, V. and Pennetta, G. (2008). hVAPB, the causative gene of a heterogeneous group of motor neuron diseases in humans, is functionally interchangeable with its Drosophila homologue DVAP-33A at the neuromuscular junction. *Hum. Mol. Genet.* **17**, 266-280.

Chen, H. J., Anagnostou, G., Chai, A., Withers, J., Morris, A., Adhikaree, J., Pennetta, G. and de Belleroche, J. S. (2010). Characterization of the properties of a novel mutation in VAPB in familial amyotrophic lateral sclerosis. *J. Biol. Chem.* **285**, 40266-40281.

Douglas, P. M., Treusch, S., Ren, H. Y., Halfmann, R., Duennwald, M. L., Lindquist, S. and Cyr, D. M. (2008). Chaperone-dependent amyloid assembly protects cells from prion toxicity. *Proc. Natl. Acad. Sci. USA* **105**, 7206-7211.

Fasana, E., Fossati, M., Ruggiano, A., Brambillasca, S., Hoogenraad, C. C., Navone, F., Francolini, M. and Borgese, N. (2010). A VAPB mutant linked to amyotrophic lateral sclerosis generates a novel form of organized smooth endoplasmic reticulum. *FASEB J.* **24**, 1419-1430.

Fink, A. L. (1998). Protein aggregation: folding aggregates, inclusion bodies and amyloid. *Fold. Des.* **3**, R9-R23.

Finley, D. (2009). Recognition and processing of ubiquitin-protein conjugates by the proteasome. *Annu. Rev. Biochem.* **78**, 477-513.

Fortun, J., Dunn, W. A., Jr, Joy, S., Li, J. and Notterpek, L. (2003). Emerging role for autophagy in the removal of aggresomes in Schwann cells. *J. Neurosci.* **23**, 10672-10680.

Foster, L. J., Weir, M. L., Lim, D. Y., Liu, Z., Trimble, W. S. and Klip, A. (2000). A functional role for VAP-33 in insulin-stimulated GLUT4 traffic. *Traffic* **1**, 512-521.

Fu, L. and Sztul, E. (2009). ER-associated complexes (ERACs) containing aggregated cystic fibrosis transmembrane conductance regulator (CFTR) are degraded by autophagy. *Eur. J. Cell Biol.* **88**, 215-226.

Funke, A. D., Esser, M., Krüttgen, A., Weis, J., Mitne-Neto, M., Lazar, M., Nishimura, A. L., Sperfeld, A. D., Trillenberg, P., Senderek, J. et al. (2010). The p.P56S mutation in the VAPB gene is not due to a single founder: the first European case. *Clin. Genet.* **77**, 302-303.

Gkogkas, C., Middleton, S., Kremer, A. M., Wardrope, C., Hannah, M., Gillingwater, T. H. and Skehel, P. (2008). VAPB interacts with and modulates the activity of ATF6. *Hum. Mol. Genet.* **17**, 1517-1526.

Ince, P. G., Highley, J. R., Kirby, J., Wharton, S. B., Takahashi, H., Strong, M. J. and Shaw, P. J. (2011). Molecular pathology and genetic advances in amyotrophic lateral sclerosis: an emerging molecular pathway and the significance of glial pathology. *Acta Neuropathol.* **122**, 657-671.

Iwata, A., Riley, B. E., Johnston, J. A. and Kopito, R. R. (2005). HDAC6 and microtubules are required for autophagic degradation of aggregated huntingtin. *J. Biol. Chem.* **280**, 40282-40292.

Kabeya, Y., Mizushima, N., Ueno, T., Yamamoto, A., Kirisako, T., Noda, T., Kominami, E., Ohsumi, Y. and Yoshimori, T. (2000). LC3, a mammalian homologue of yeast Apg8p, is localized in autophagosome membranes after processing. *EMBO J.* **19**, 5720-5728.

Kaiser, S. E., Brickner, J. H., Reilein, A. R., Fenn, T. D., Walter, P. and Brunger, A. T. (2005). Structural basis of FFAT motif-mediated ER targeting. *Structure* **13**, 1035-1045.

Kanekura, K., Nishimoto, I., Aiso, S. and Matsuoka, M. (2006). Characterization of amyotrophic lateral sclerosis-linked P56S mutation of vesicle-associated membrane protein-associated protein B (VAPB/ALS8). *J. Biol. Chem.* **281**, 30223-30233.

Kawaguchi, Y., Kovacs, J. J., McLaurin, A., Vance, J. M., Ito, A. and Yao, T. P. (2003). The deacetylase HDAC6 regulates aggresome formation and cell viability in response to misfolded protein stress. *Cell* **115**, 727-738.

Kawano, M., Kumagai, K., Nishijima, M. and Hanada, K. (2006). Efficient trafficking of ceramide from the endoplasmic reticulum to the Golgi apparatus requires a VAMP-associated protein-interacting FFAT motif of CERT. *J. Biol. Chem.* **281**, 30279-30288.

Kim, S., Leal, S. S., Ben Halevy, D., Gomes, C. M. and Lev, S. (2010). Structural requirements for VAP-B oligomerization and their implication in amyotrophic lateral sclerosis-associated VAP-B(P56S) neurotoxicity. *J. Biol. Chem.* **285**, 13839-13849.

Kirkin, V., McEwan, D. G., Novak, I. and Dikic, I. (2009). A role for ubiquitin in selective autophagy. *Mol. Cell* **34**, 259-269.

Komatsu, M., Waguri, S., Koike, M., Sou, Y. S., Ueno, T., Hara, T., Mizushima, N., Iwata, J., Ezaki, J., Murata, S. et al. (2007). Homeostatic levels of p62 control cytoplasmic inclusion body formation in autophagy-deficient mice. *Cell* **131**, 1149-1163.

Kopito, R. R. (2000). Aggresomes, inclusion bodies and protein aggregation. *Trends Cell Biol.* **10**, 524-530.

Kremer, J. R., Mastronarde, D. N. and McIntosh, J. R. (1996). Computer visualization of three-dimensional image data using IMOD. *J. Struct. Biol.* **116**, 71-76.

Kuusisto, E., Salminen, A. and Alafuzoff, I. (2001). Ubiquitin-binding protein p62 is present in neuronal and glial inclusions in human tauopathies and synucleinopathies. *Neuroreport* 12, 2085-2090.

Lev, S., Ben Halevy, D., Peretti, D. and Dahan, N. (2008). The VAP protein family: from cellular functions to motor neuron disease. *Trends Cell Biol.* 18, 282-290.

Lingwood, D., Schuck, S., Ferguson, C., Gerl, M. J. and Simons, K. (2009). Generation of cubic membranes by controlled homotypic interaction of membrane proteins in the endoplasmic reticulum. *J. Biol. Chem.* 284, 12041-12048.

Loewen, C. J. and Levine, T. P. (2005). A highly conserved binding site in vesicle-associated membrane protein-associated protein (VAP) for the FFAT motif of lipid-binding proteins. *J. Biol. Chem.* 280, 14097-14104.

Loewen, C. J., Roy, A. and Levine, T. P. (2003). A conserved ER targeting motif in three families of lipid binding proteins and in Opi1p binds VAP. *EMBO J.* 22, 2025-2035.

Mastronarde, D. N. (1997). Dual-axis tomography: an approach with alignment methods that preserve resolution. *J. Struct. Biol.* 120, 343-352.

Mitne-Neto, M., Machado-Costa, M., Marchetto, M. C., Bengtson, M. H., Joazeiro, C. A., Tsuda, H., Bellen, H. J., Silva, H. C., Oliveira, A. S., Lazar, M. et al. (2011). Downregulation of VAPB expression in motor neurons derived from induced pluripotent stem cells of ALS8 patients. *Hum. Mol. Genet.* 20, 3642-3652.

Moumen, A., Virard, I. and Raoul, C. (2011). Accumulation of wildtype and ALS-linked mutated VAPB impairs activity of the proteasome. *PLoS ONE* 6, e26066.

Nagaoka, U., Kim, K., Jana, N. R., Doi, H., Maruyama, M., Mitsui, K., Oyama, F. and Nukina, N. (2004). Increased expression of p62 in expanded polyglutamine-expressing cells and its association with polyglutamine inclusions. *J. Neurochem.* 91, 57-68.

Nishimura, A. L., Al-Chalabi, A. and Zatz, M. (2005). A common founder for amyotrophic lateral sclerosis type 8 (ALS8) in the Brazilian population. *Hum. Genet.* 118, 499-500.

Nishimura, A. L., Mitne-Neto, M., Silva, H. C. A., Richieri-Costa, A., Middleton, S., Cascio, D., Kok, F., Oliveira, J. R. M., Gillingwater, T., Webb, J. et al. (2004). A mutation in the vesicle-trafficking protein VAPB causes late-onset spinal muscular atrophy and amyotrophic lateral sclerosis. *Am. J. Hum. Genet.* 75, 822-831.

Olzmann, J. A. and Chin, L. S. (2008). Parkin-mediated K63-linked polyubiquitination: a signal for targeting misfolded proteins to the aggresome-autophagy pathway. *Autophagy* 4, 85-87.

Olzscha, H., Schermann, S. M., Woerner, A. C., Pinkert, S., Hecht, M. H., Tartaglia, G. G., Vendruscolo, M., Hayer-Hartl, M., Hartl, F. U. and Vabulas, R. M. (2011). Amyloid-like aggregates sequester numerous metastable proteins with essential cellular functions. *Cell* 144, 67-78.

Pankiv, S., Clausen, T. H., Lamark, T., Brech, A., Bruun, J. A., Outzen, H., Øvervatn, A., Bjørkøy, G. and Johansen, T. (2007). p62/SQSTM1 binds directly to Atg8/LC3 to facilitate degradation of ubiquitinated protein aggregates by autophagy. *J. Biol. Chem.* 282, 24131-24145.

Peretti, D., Dahan, N., Shimoni, E., Hirschberg, K. and Lev, S. (2008). Coordinated lipid transfer between the endoplasmic reticulum and the Golgi complex requires the VAP proteins and is essential for Golgi-mediated transport. *Mol. Biol. Cell* 19, 3871-3884.

Prosser, D. C., Tran, D., Gougeon, P. Y., Verly, C. and Ngsee, J. K. (2008). FFAT rescues VAPA-mediated inhibition of ER-to-Golgi transport and VAPB-mediated ER aggregation. *J. Cell Sci.* 121, 3052-3061.

Puhka, M., Vihinen, H., Joensuu, M. and Jokitalo, E. (2007). Endoplasmic reticulum remains continuous and undergoes sheet-to-tubule transformation during cell division in mammalian cells. *J. Cell Biol.* 179, 895-909.

Rabinovich, E., Kerem, A., Fröhlich, K. U., Diamant, N. and Bar-Nun, S. (2002). AAA-ATPase p97/Cdc48p, a cytosolic chaperone required for endoplasmic reticulum-associated protein degradation. *Mol. Cell. Biol.* 22, 626-634.

Ratnaparkhi, A., Lawless, G. M., Schweizer, F. E., Golshani, P. and Jackson, G. R. (2008). A Drosophila model of ALS: human ALS-associated mutation in VAP33A suggests a dominant negative mechanism. *PLoS ONE* 3, e2334.

Ravikumar, B. and Rubinsztein, D. C. (2004). Can autophagy protect against neurodegeneration caused by aggregate-prone proteins? *Neuroreport* 15, 2443-2445.

Ravikumar, B., Duden, R. and Rubinsztein, D. C. (2002). Aggregate-prone proteins with polyglutamine and polyalanine expansions are degraded by autophagy. *Hum. Mol. Genet.* 11, 1107-1117.

Rocha, N., Kuijl, C., van der Kant, R., Janssen, L., Houben, D., Janssen, H., Zwart, W. and Neefjes, J. (2009). Cholesterol sensor ORP1L contacts the ER protein VAP to control Rab7-RILP-p150 Glued and late endosome positioning. *J. Cell Biol.* 185, 1209-1225.

Ross, C. A. and Pickart, C. M. (2004). The ubiquitin-proteasome pathway in Parkinson's disease and other neurodegenerative diseases. *Trends Cell Biol.* 14, 703-711.

Ross, C. A. and Poirier, M. A. (2004). Protein aggregation and neurodegenerative disease. *Nat. Med.* 10 Suppl, S10-S17.

Saita, S., Shirane, M., Natume, T., Iemura, S. and Nakayama, K. I. (2009). Promotion of neurite extension by protrudin requires its interaction with vesicle-associated membrane protein-associated protein. *J. Biol. Chem.* 284, 13766-13777.

Selkoe, D. J. (2003). Folding proteins in fatal ways. *Nature* 426, 900-904.

Shi, J., Lua, S., Tong, J. S. and Song, J. (2010). Elimination of the native structure and solubility of the hVAPB MSP domain by the Pro56Ser mutation that causes amyotrophic lateral sclerosis. *Biochemistry* 49, 3887-3897.

Skehel, P. A., Martin, K. C., Kandel, E. R. and Bartsch, D. (1995). A VAMP-binding protein from Aplysia required for neurotransmitter release. *Science* 269, 1580-1583.

Snapp, E. L., Hegde, R. S., Francolini, M., Lombardo, F., Colombo, S., Pedrazzini, E., Borgese, N. and Lippincott-Schwartz, J. (2003). Formation of stacked ER cisternae by low affinity protein interactions. *J. Cell Biol.* 163, 257-269.

Soussan, L., Burakov, D., Daniels, M. P., Toister-Achituv, M., Porat, A., Yarden, Y. and Elazar, Z. (1999). ERG30, a VAP-33-related protein, functions in protein transport mediated by COPI vesicles. *J. Cell Biol.* 146, 301-312.

Stefan, C. J., Manford, A. G., Baird, D., Yamada-Hanff, J., Mao, Y. and Emr, S. D. (2011). Osh proteins regulate phosphoinositide metabolism at ER-plasma membrane contact sites. *Cell* 144, 389-401.

Suzuki, H. and Matsuoka, M. (2011). Amyotrophic lateral sclerosis-linked mutant VAPB enhances TDP-43-induced motor neuronal toxicity. *J. Neurochem.* 119, 1099-1107.

Suzuki, H., Kanekura, K., Levine, T. P., Kohno, K., Olkkonen, V. M., Aiso, S. and Matsuoka, M. (2009). ALS-linked P56S-VAPB, an aggregated loss-of-function mutant of VAPB, predisposes motor neurons to ER stress-related death by inducing aggregation of co-expressed wild-type VAPB. *J. Neurochem.* 108, 973-985.

Tanaka, M., Kim, Y. M., Lee, G., Junn, E., Iwatsubo, T. and Mouradian, M. M. (2004). Aggresomes formed by alpha-synuclein and synphilin-1 are cytoprotective. *J. Biol. Chem.* 279, 4625-4631.

Teuling, E., Ahmed, S., Haasdijk, E., Demmers, J., Steinmetz, M. O., Akhmanova, A., Jaarsma, D. and Hoogenraad, C. C. (2007). Motor neuron disease-associated mutant vesicle-associated membrane protein-associated protein (VAP) B recruits wild-type VAPs into endoplasmic reticulum-derived tubular aggregates. *J. Neurosci.* 27, 9801-9815.

Tsuda, H., Han, S. M., Yang, Y., Tong, C., Lin, Y. Q., Mohan, K., Haueter, C., Zoghbi, A., Harati, Y., Kwan, J. et al. (2008). The amyotrophic lateral sclerosis 8 protein VAPB is cleaved, secreted, and acts as a ligand for Eph receptors. *Cell* 133, 963-977.

Tudor, E. L., Galtrey, C. M., Perkinton, M. S., Lau, K. F., De Vos, K. J., Mitchell, J. C., Ackerley, S., Hortobágyi, T., Vámos, E., Leigh, P. N. et al. (2010). Amyotrophic lateral sclerosis mutant vesicle-associated membrane protein-associated protein-B transgenic mice develop TAR-DNA-binding protein-43 pathology. *Neuroscience* 167, 774-785.

Wakana, Y., Takai, S., Nakajima, K., Tani, K., Yamamoto, A., Watson, P., Stephens, D. J., Hauri, H. P. and Tagaya, M. (2008). Bap31 is an itinerant protein that moves between the peripheral endoplasmic reticulum (ER) and a juxtanuclear compartment related to ER-associated Degradation. *Mol. Biol. Cell* 19, 1825-1836.

Webb, J. L., Ravikumar, B., Atkins, J., Skepper, J. N. and Rubinsztein, D. C. (2003). Alpha-Synuclein is degraded by both autophagy and the proteasome. *J. Biol. Chem.* 278, 25009-25013.

Ye, Y., Meyer, H. H. and Rapoport, T. A. (2001). The AAA ATPase Cdc48/p97 and its partners transport proteins from the ER into the cytosol. *Nature* 414, 652-656.

Zatloukal, K., Stumptner, C., Fuchsbichler, A., Heid, H., Schnoelzer, M., Kenner, L., Kleinert, R., Prinz, M., Aguzzi, A. and Denk, H. (2002). p62 Is a common component of cytoplasmic inclusions in protein aggregation diseases. *Am. J. Pathol.* 160, 255-263.